Estimates for Helium Cooling of a Modular DEMO First Wall

W. Daenner

IPP 2/258 July 1982

MAX-PLANCK-INSTITUT FÜR PLASMAPHYSIK

8046 GARCHING BEI MÜNCHEN

MAX-PLANCK-INSTITUT FÜR PLASMAPHYSIK

GARCHING BEI MÜNCHEN

Estimates for Helium Cooling of a Modular DEMO First Wall

W. Daenner

IPP 2/258 July 1982

Die nachstehende Arbeit wurde im Rahmen des Vertrages zwischen dem Max-Planck-Institut für Plasmaphysik und der Europäischen Atomgemeinschaft über die Zusammenarbeit auf dem Gebiete der Plasmaphysik durchgeführt.

Abstract

Lifetime studies performed for a modular first wall of a DEMO reactor with 2 MW/m^2 neutron wall loading have shown a strong impact of the temperature level at which the wall is operated. This result stimulated closer investigation of the cooling problem. On the basis of helium gas as the coolant, two alternative concepts of cooling the first wall are analyzed which conform to the design requirements imposed by the geometrical restrictions prescribed by the FWLTB life prediction code. In the investigation emphasis is placed on the hemispherical cap which closes a cylindrical cell at the side exposed to the plasma. This cap and a smaller concentric one provide an annular gap in which the coolant flows.

In the one concept the coolant is assumed to enter the gap at the bottom of the hemisphere and subsequently to flow upwards along the increasing surface of the hemisphere with decreasing velocity or vice versa. The second concept assumes an essentially rectangular channel wound around the hemisphere inside the annular gap. For both concepts calculations have yielded the coolant-side wall temperatures as a function of the first-wall thickness and the fraction of α-power delivered to the wall. While the first concept revealed acceptable temperatures only within a narrow parameter range, the second showed a much higher cooling capacity. To summarize, the results demonstrate that it should be possible to keep the wall temperatures at or below 500°C, depending on the parameters chosen.

Contents

1. Introduction

At the 3rd INTOR Workshop (Phase IIa) [1] just a few parameters have been specified for the DEMO power plant envisaged to succeed INTOR as the next step towards a commercial reactor. According to these specifications DEMO should operate at a neutron wall loading of about 2 MW/m^2 and with burn times longer than 1000 s. The thermal and gross electric power are envisaged at around 1 GW and 300 MW respectively. To ensure that the first wall adequately meets demonstration standards, a fluence target of 10 - 15 $MW\text{-}yr/m^2$ was set.

With regard to the irradiation test facilities now available and the test capabilities of INTOR, it has been recognized that it is only nickel - containing alloys, particularly the austenitic stainless steel 316 SS, that afford a sufficiently reliable data base to qualify as the first wall and structural materials in DEMO. It depends to some extent on the outcome of this test programme whether the postulated fluence goal can really be achieved. In addition, the design and operation conditions of the DEMO reactor first wall will have a significant impact.

Within the frame set by the few parameters quoted above some scoping studies have been performed with the FWLTB life prediction code, which was developed at IPP Garching.

These studies have shown [2] that the erosion rates to be expected in a DEMO govern the lifetime of the first wall. The erosion rate and fluence goal determine the necessary thickness of the first wall at the beginning of operation. The higher this initial wall thickness has to be chosen, the higher are the thermal stresses across the wall; they also strongly depend on the fraction of the α-power impinging on the wall. These stresses are the main reason for life termination according to a criterion in which the time rupture life is involved. This in turn is, however, a strong function of the temperature level at which the wall is operated. Undoubtedly, the useful life due to this criterion is the higher the lower the wall temperatures can be kept. This result quite generally calls for realizing the concept of a "cool wall" where "cool" still means, temperatures of about 300 to 350°C below which other limitations (swelling and ductility) for the wall-life exist.

Hence in this paper we examine the cooling system requirements which lead to an acceptable coolant side wall temperature. The coolant is assumed here to be helium streaming under turbulent flow conditions. This choice is governed by the fact, that helium affords advantages over, for instance, liquid lithium and water as regards safety. The modular concept, on the other hand, was chosen such as to fit as closely as possible into the frame prescribed by the FWLTB life prediction code, which calls for cylindrical or spherical elements. In this way a satisfactory degree of consistency is maintained.

2. The module concept

Since the FWLTB life prediction code is designed exclusively for cylindrical and spherical elements, we consider a module concept which is in line with this restriction. It is shown in Fig. 1.

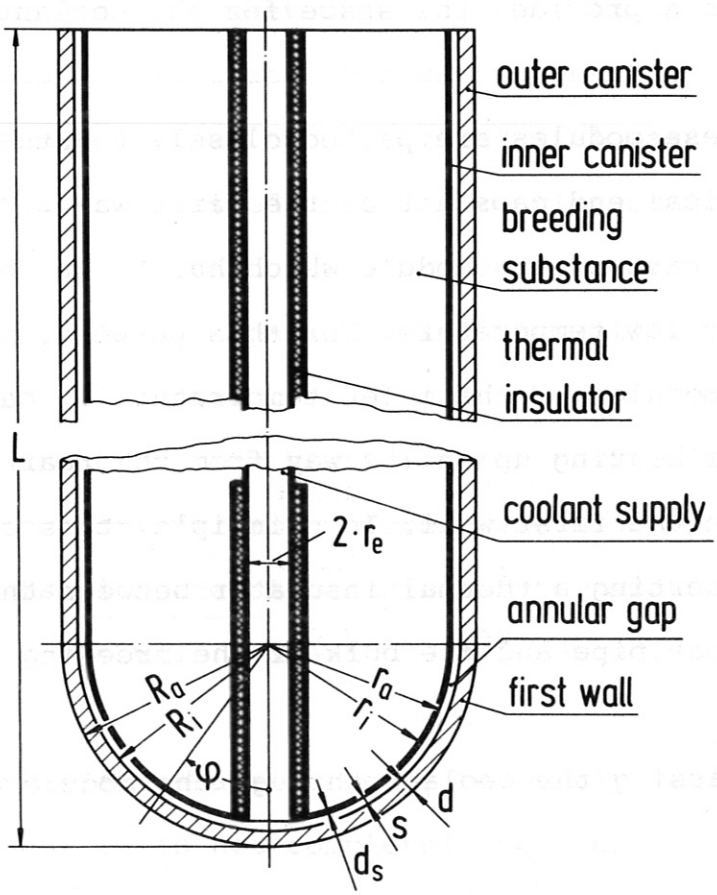

Fig. 1: Schematic representation of the module investigated

The outer enclosure is represented by a cylindrical canister of radius R_a closed by a hemispherical cap of the same radius. The wall thickness d of the canister is assumed to be the same at all locations and to be determined by lifetime considerations only. The outer canister is assumed to enclose a second canister of thickness d_s for containing the breeding material. Between the outer and inner canisters a gap of width s provides the space for the coolant flow.

If many of these modules are packed closely together, only the hemispherical end caps act as the first wall. This is therefore the part of the module which has to be kept at a sufficiently low temperature. For this purpose, helium entering the module with the inlet temperature θ_i has to be prevented from heating up on its way from the rear of the module down to the first wall. In principle, this could be done by inserting a thermal insulator between the coolant entrance pipe and the bulk of the breeding substance.

Two ways of passing the coolant through the module are conceivable:

a) The cold helium enters the module through the central tube, enters the gap at the tip of the module, flows along the hemispherical annular gap, and leaves it along the cylindrical surfaces of the two canisters.

b) The second possibility is just to pass the helium in the opposite direction.

As will be shown later, the second approach is the more favourable one with respect to the wall temperature. Since the flow cross-section increases with increasing distance from the module tip, the flow velocity accordingly decreases. As a consequence the heat transfer coefficient decreases, too, and becomes smallest at the location where the coolant crosses from the hemispherical to the cylindrical part of the module. If the coolant is passed in the direction of increasing flow cross-section, low heat transfer coefficients coincide with the higher coolant temperature and the wall temperatures become high. If, however, the coolant is passed in the opposite direction, low heat transfer coefficients coincide with the low coolant temperatures, and high heat transfer coefficients with the higher coolant temperatures. In this way the maximum wall temperature is reduced.

In fact, this advantage can only be partly realized. It should be noted that it is not completely possible to keep the coolant at the inlet temperature until it reaches any point of the hemispherical cap. It will at least take up the heat from the surrounding pipe. If the helium enters through the central pipe, a thin-walled pipe and a small surface can ensure a modest temperature increase. If it enters along the surface of

the outer canister, both wall thickness and surface area are much higher, which leads to a much higher coolant temperature at the entrance of the gap. In addition, the amount of insulator material needed is very different, as may also be the difficulty in manufacturing it and maintaining its integrity.

Of course, modifications of these two concepts of passing the coolant to the first wall are conceivable. All solutions, however, entail great complexity of design and only lead to modest improvements of the wall temperatures. As analysis will show, the real problem is the appropriate way of cooling the first wall itself. For this reason an additional concept based on a rectangular channel wound within the hemispherical annular gap is proposed and analyzed. In this way, coolant velocities and hence heat transfer coefficients can be kept approximately constant, which leads to a significant improvement with respect to the maximum wall temperatures to be expected.

3. Analysis of the module power

3.1. Module power and mass flow rate

The module exposes to the plasma an area

$$F_p = \pi \cdot R_a^2 \quad , \tag{1}$$

where R_a is the outer radius. The total thermal power produced inside the module by neutron and gamma reactions, P_n, can be calculated from the neutron wall load q_n and the energy multiplication factor of the blanket M:

$$P_n = q_n \cdot M \cdot F_p \quad . \tag{2}$$

In addition to this nuclear power, the module is exposed to an external heat flux which ultimately stems from that fraction of the thermonuclear reaction power which was delivered to the α-particles. For the D-T reaction assumed the maximum heat flux density q_α is given by

$$q_\alpha = 0.25 \cdot q_n \quad . \tag{3}$$

Depending on the exhaust concept chosen for the reactor, only a certain fraction α will impinge on the wall, the remainder being passed to another component such as a

divertor or a limiter. Hence the total power P_α from the α-particle source which hits the wall is

$$P_\alpha = \alpha \cdot q_\alpha \cdot F_p = 0.25 \cdot \alpha \cdot q_n \cdot F_p \quad . \qquad (4)$$

In order to get the total thermal power P_{th} of the module, we have to add eqs. (2) and (4).Observing eq. (3), we obtain

$$P_{th} = F_p \cdot q_n \cdot (M + 0.25 \cdot \alpha). \qquad (5)$$

This power has to be transferred to the coolant, which necessitates a mass flow rate $\dot{m}$

$$\dot{m} = \frac{P_{th}}{c_p(\Theta_o - \Theta_i)} \quad . \qquad (6)$$

3.2. Power released in the module head

Only part of the total module power P_{th} is released within the head of the module, upon which we now focus attention. We define as the head of the module the entire volume of the hemispherical cap which is enclosed by the "first wall".

In any case, the total power P_α , eq. (4), is transferred to the head and has to be cooled away. Of the total nuclear heat P_n only a fraction is produced in the head. We describe this

fraction using the mean power density over the volume of the different parts of the module head, neglecting any spatial dependence.

The volume of the first wall V_w is given by

$$V_w = \frac{2}{3} \pi (R_a^3 - R_i^3) \quad , \tag{7}$$

where

$$R_i = R_a - d \quad . \tag{8}$$

The volume of the hemispherical part of the second canister, which contains the breeding material, is given by

$$V_s = \frac{2}{3} \pi (r_a^3 - r_i^3) - \pi r_e^2 \cdot d_s \quad , \tag{9}$$

where

$$r_a = R_a - d - s \tag{10}$$

and

$$r_i = r_a - d_s \quad . \tag{11}$$

The second term in eq. (9) describes the hole in the containment shell, the radius of which is that of the coolant entry pipe r_e.

The volume of the breeding substance within the head is described by

$$V_B = \frac{2}{3} \pi r_i^3 - \pi \circ r_e^2 \cdot r_i \quad . \tag{12}$$

In this equation, V_B also contains the volume contributed by the wall of the entry pipe and by the insulator material. It is assumed that the power produced within these components does not have a great influence on the overall power density within V_B, which should be governed by the breeding substance.

The actual power densities within these three volumes Q_w, Q_s, and Q_B are coupled to the neutron wall loading q_n and may be taken from appropriate neutronics calculations as is the energy multiplication factor M. With the external heat load P_α taken into account, the total power released within the module head, P_H, may now be expressed as

$$P_H = P_\alpha + Q_w \cdot V_w + Q_s \cdot V_s + Q_B \cdot V_B \quad . \tag{13}$$

It is useful to relate this power to the total thermal power of the module by defining

$$\beta = \frac{P_H}{P_{th}} \quad . \tag{14}$$

3.3. Heat flux densities at the channel surfaces

According to the concept described so far the coolant streaming within the hemispherical annular gap is heated from two sides. For simplicity, we assume a homogeneous heat flux density at the channel surfaces, which requires essentially radial heat transport within the various components.

The outer channel surface F_o is given by

$$F_o = 2\pi \cdot R_i^2 \quad , \tag{15}$$

the inner one, F_i, by

$$F_i = 2\pi \cdot r_a^2 - \pi r_e^2 \quad , \tag{16}$$

again taking into account the hole in the second canister to admit the coolant entry pipe. While P_α and the nuclear heat generated within the first wall, P_w, has to be transferred across the outer surface:

$$P_o = P_\alpha + V_w \cdot Q_w \quad , \tag{17}$$

the inner surface is loaded by

$$P_i = V_s \cdot Q_s + V_B \cdot Q_B \quad . \tag{18}$$

The corresponding heat flux densities p_o and p_i thus become

$$p_o = \frac{P_\alpha + V_w \cdot Q_w}{2\pi R_i^2} , \tag{19}$$

$$p_i = \frac{V_s \cdot Q_s + V_B \cdot Q_B}{2\pi r_a^2 - \pi r_e^2} . \tag{20}$$

4. The annular gap concept

In this section we confine ourselves to analysis of the concept by which the coolant enters through the central pipe, enters the hemispherical cap at the tip of the module and flows homogeneously along the first wall in the annular gap between the outer and inner canisters.

4.1. Analysis of the concept

The characteristic feature of the annular gap concept is that the coolant velocity w changes when proceeding in the flow direction. These changes are due to the variation of the flow cross-section on the one hand and to the increase of the coolant temperature on the other hand. We therefore introduce the angle φ as a variable as defined in Fig. 1.

The mean channel radius R_c and the gap cross-section A_c vary with φ as

$$R_c(\varphi) = R_{c\infty} \cdot \sin\varphi \quad , \tag{21}$$

$$A_c(\varphi) = A_{c\infty} \cdot \sin\varphi \quad , \tag{22}$$

where $R_{c\infty}$ and $A_{c\infty}$ are the channel radius and the gap cross-section at the exit of the hemisphere:

$$R_{c\infty} = R_a - d - \frac{s}{2} \quad , \tag{23}$$

$$A_{c\infty} = 2\pi \cdot R_{c\infty} \cdot s \quad . \tag{24}$$

From the mass flow rate as defined by eq. (6) we find the volume flow rate $\dot{V}$ and the coolant velocity w:

$$V(\varphi) = \frac{\dot{m}}{\rho\,[\theta(\varphi)]} \quad , \tag{25}$$

$$w(\varphi) = \frac{\dot{m}}{\rho[\theta(\varphi)] \cdot A_{c\infty} \cdot \sin\varphi} \quad . \tag{26}$$

In these equations $\rho[\theta(\varphi)]$ is the local coolant density which varies as the temperature θ increases, this in turn being a function of the angle φ. In order to determine $\theta(\varphi)$, we have to examine the amount of heat transferred to the coolant up to angle φ.

For a certain interval $d\varphi$ the heat transfer surface areas at the outside and inside of the gap are

$$df_o = 2\pi \cdot R_i^2 \cdot \sin\varphi \; d\varphi \quad , \tag{27}$$

$$df_i = 2\pi \cdot r_a^2 \cdot \sin\varphi \; d\varphi \quad . \tag{28}$$

For the total heat P absorbed by the coolant up to angle φ it follows that

$$P(\varphi) = \int p_o \, df_o + \int p_i \, df_i \quad . \tag{29}$$

The integration boundaries for the two contributions are different because the heat transfer from the inner surface starts at an angle φ_e which is dependent on the radius r_e of the central entrance pipe: It approximately holds that

$$\varphi_e = \text{arc sin} \left(\frac{r_e}{R_{c\infty}} \right) \quad . \tag{30}$$

Using eq. (30), and introducing eqs. (27) and (28), eq. (29) becomes

$$P(\varphi) = 2\pi R_i^2 p_o \int_0^{\varphi} \sin\varphi \, d\varphi + 2\pi r_a^2 \cdot p_i \int_{\varphi_e}^{\varphi} \sin\varphi \, d\varphi \tag{31}$$

or

$$P(\varphi) = 2\pi R_i^2 p_o (1 - \cos\varphi) + 2\pi r_a^2 p_i (\cos\varphi_e - \cos\varphi) \quad . \tag{32}$$

With this equation we calculate the local coolant temperature

$$\Theta(\varphi) = \Theta_i + \frac{P(\varphi)}{m \cdot c_p} \quad . \tag{33}$$

In order to find the wall temperature $\vartheta_o(\varphi)$, we have to know the heat transfer coefficient h_o. This is obtained from the Nusselt number Nu:

$$h_o(\varphi) = \frac{k[\vartheta_F(\varphi)]}{d_H} \cdot Nu(\varphi) \quad , \tag{34}$$

in which k is the thermal conductivity of the coolant and d_H the hydraulic diameter. For an annular gap d_H is twice the gap width:

$$d_H = 2 \cdot s \quad . \tag{35}$$

The Nusselt number Nu in the case of helium cooling is obtained from

$$Nu(\varphi) = 0.023 \quad R_e(\varphi)^{0.8} \quad Pr(\varphi)^{0.8} \quad , \tag{36}$$

where the Reynolds number Re and the Prandtl number Pr are given by

$$Re(\varphi) = \frac{w(\varphi) \cdot d_H \cdot \rho[\vartheta_F(\varphi)]}{\mu[\vartheta_F(\varphi)]} \quad , \tag{37}$$

$$Pr(\varphi) = \frac{c_p[\vartheta_F(\varphi) \cdot \mu[\vartheta_F(\varphi)]}{k[\vartheta_F(\varphi)]} \quad . \tag{38}$$

The coolant properties, viz. the density ρ, the specific heat c_p, the thermal conductivity k, and the dynamic viscosity μ, have to be calculated for the average film temperature ϑ_F, which follows from

$$\vartheta_F(\varphi) = \frac{1}{2}\,[\theta(\varphi) + \vartheta_o(\varphi)] \tag{39}$$

and needs iterative calculation.

The first-wall temperature $\vartheta_o(\varphi)$ is finally found from

$$\vartheta_o(\varphi) = \theta(\varphi) + \frac{p_o}{h_o(\varphi)} \tag{40}$$

In the same way the wall temperature of the inner canister is found by replacing p_o by p_i:

$$\vartheta_i(\varphi) = \theta(\varphi) + \frac{p_i}{h_i(\varphi)} \tag{41}$$

The same iteration procedure has to be applied to arrive at $h_i(\varphi)$ as was used to obtain $h_o(\varphi)$.

4.2. Numerical results

The procedure described above was applied to a number of parameter combinations which are consistent with the FWLTB lifetime studies performed for the DEMO [2]. The prescribed neutron wall loading of $q_n = 2$ MW/m^2 gives rise to a nuclear power density within the first wall of about $Q_w = 20$ W/cm^3. The same value was assumed for the inner canister, $Q_s = 20$ W/cm^3. Since no breeding material had yet been specified, we chose numbers valid for liquid lithium [3]. Near the first wall a power density of about $Q_B = 6$ W/cm^3 has to be expected, while the energy multiplication factor is around $M = 1.13$ for a blanket of 1 m thickness. The helium pressure was assumed to be $p_c = 4$ MPa. In order to allow a reasonable thermal efficiency of the steam power cycle, the coolant inlet and outlet temperatures were chosen to be $\Theta_i = 300^{\circ}$C and $\Theta_o = 500^{\circ}$C, respectively. The size of the module was specified by its outer radius $R_a = 5$ cm. While the first-wall thickness d was subjected to variation, fixed values were used for the gap width s, the wall thickness of the inner canister d_s, and the radius of the central entrance pipe r_e: $s = 0.15$ cm; $d_s = 0.1$ cm, and $r_e = 0.5$ cm. All helium property data were taken from [4].

The first-wall thickness d and the parameter α describing the fraction of α-power delivered to the first wall were varied in the study. In order to cover the same ranges as in the case of the FWLTB calculations, d was varied within the limits 0.2 and 1.6 cm, α within 0 and 1.0.

Independently of the wall thickness d, the total thermal power of a module varies from 17.7 kW for α = 0 to 21.6 kW for α = 1. Accordingly, the necessary mass flow rates vary from about 60 kg/h to about 75 kg/h. The coolant velocities at the gap entrance range between 110 and 133 m/s and drop to about 12 to 22 m/s at the gap exit. The Reynolds number calculated for the lowest coolant velocity shows that the flow conditions are already rather close to the point where transition from turbulent to laminar conditions occurs. While the heat transfer coefficients in the high-velocity region range between 0.75 and 0.8 W/cm^2K, they drop to about 0.12 W/cm^2K at the gap exit. Of course, this gives rise to large film temperature gradients within the flow boundary layer.

While the numbers reported above do not vary too much with d and α, the resulting wall temperatures ϑ_o do. This is due to the effect that the coolant temperatures increase to different values because the power transferred via the outside surface of the coolant gap significantly varies with d and α. The quantity β defined in eq. (14) is a measure of it.

It describes not only the fraction of the total thermal power generated within the module head but also the fraction of the coolant temperature rise $\Delta\Theta_c/(\Theta_o - \Theta_i)$ within the hemispherical annular gap. Its dependence on d and α is shown in Fig. 2. The value of $\Delta\Theta_c$ can be read directly

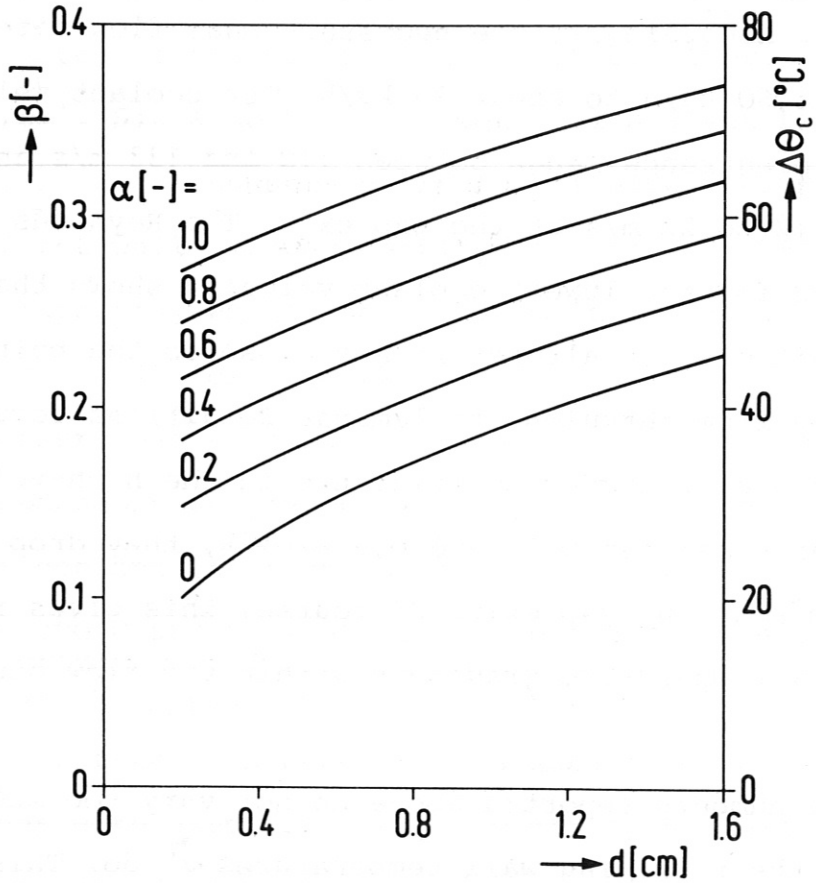

Fig. 2: The ratio β of the power released in the module head and the total module power, and the coolant temperature rise $\Delta\Theta_c$ in the module head as a function of wall thickness d and fractional α-power α.

from the scale at the right hand side of this diagram. According to this figure, the coolant temperature rise within the hemispherical annular gap ranges between 20°C and 74°C, depending on the values for d and α chosen.

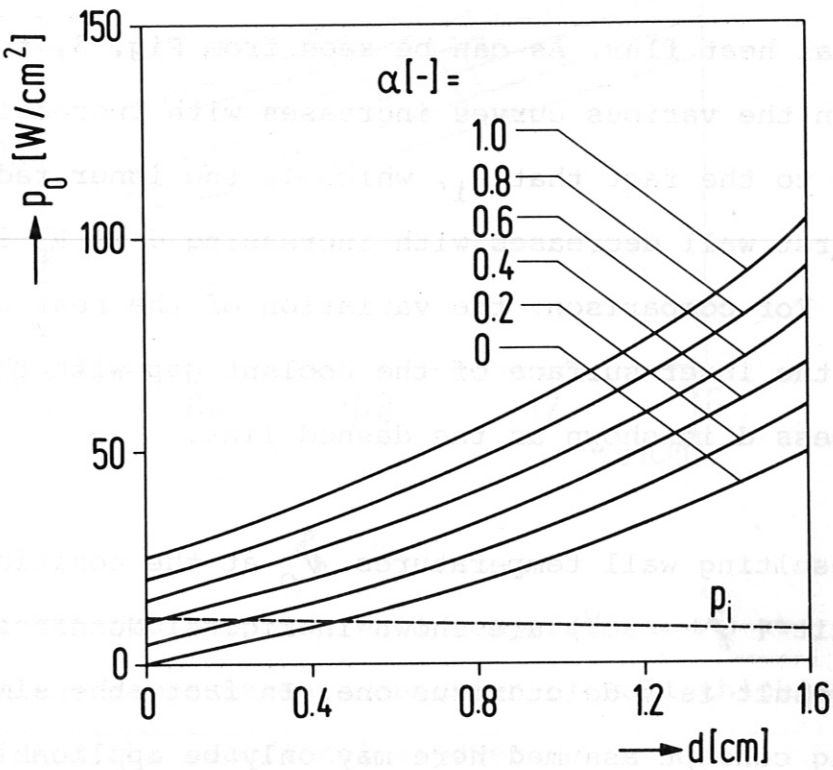

Fig. 3: Heat flux density p_o at the outer surface of the gap as a function of wall thickness d and fractional α-power α.

Figure 3 shows the heat flux density p_o at the outer surface of the coolant gap as a function of the first-wall thickness d for various values of α. The curve designated as $\alpha = 0$ represents the contribution of nuclear heating within the first wall, while the others additionally include the external heat flux. As can be seen from Fig. 3, the distance between the various curves increases with increasing d. This is due to the fact that R_i, which is the inner radius of the first wall decreases with increasing d if R_a is kept fixed. For comparison, the variation of the heat flux density p_i at the inner surface of the coolant gap with the wall thickness d is shown as the dashed line.

The resulting wall temperatures ϑ_o at the position of the gap exit ($\varphi = 90^o$) are shown in Fig. 4. Needless to say, this result is a deleterious one. In fact, the simple cooling concept assumed here may only be applicable if the fraction of α-power delivered to the wall is extremely small and thin walls can be used. The latter calls for a very low erosion rate.

Matters may improve a little bit, but not fundamentally, if the module or coolant parameters are changed. Choosing a lower inlet temperature Θ_i, for instance, only has a beneficial effect if d and α are small. At higher values,

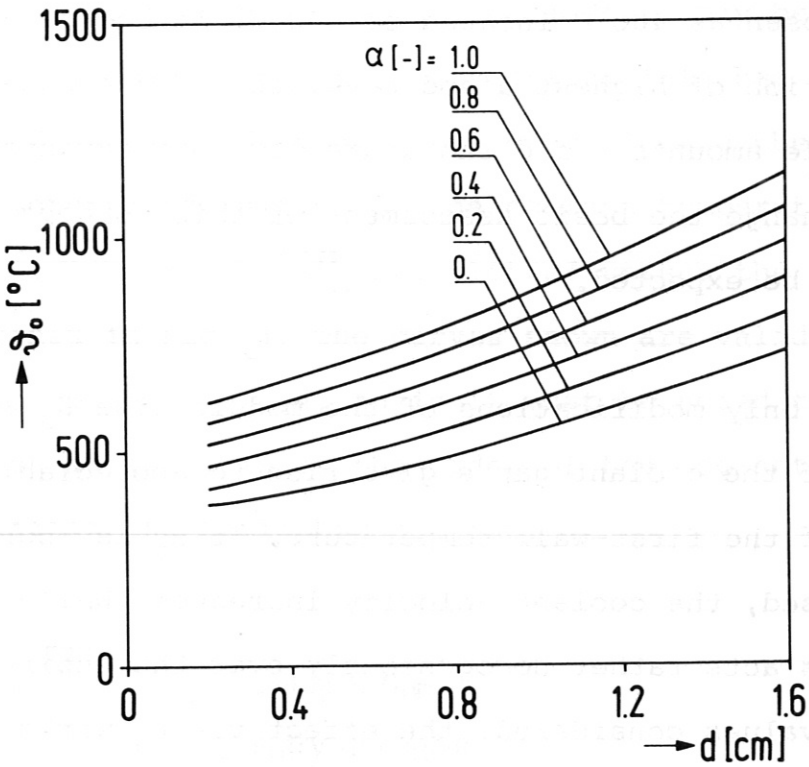

Fig. 4: The coolant-side wall temperature ϑ_o at the gap exit as a function of wall thickness d and the fractional α-power α.

the correspondingly lower mass flow rates and coolant velocities give rise to lower heat transfer coefficients. The resulting larger film temperatures gradients override the effect of the lower coolant temperature.

It is more advantageous to lower the outlet temperature θ_o. The maximum gain with respect to wall temperatures is about

100°C within the range of d and α-values considered if θ_o is chosen as 480°C instead of 500°C. It occurs at the combination of highest d and α values and decreases to negligible amounts if d and α are low. Big advantages which may change the basic assessment of this concept are thus not to be expected.

In general, only modifications of the module size R_a and/or the width of the coolant gap s give rise to appreciable decreases of the first-wall temperature. If R_a is increased or s decreased, the coolant velocity increases. While the effect via s acts rather homogeneously over the entire range of d and α-values considered, the effect via R_a works well almost only in the case of thick walls and high values of α. At low values even the opposite effect may occur. In principal, it seems possible to get the wall temperatures down to about 500°C to 600°C if either of the two means is applied. It should be noted, however, that a gap width below 0.15 cm may already raise difficulties with regard to the problem of dimensional stability due to swelling and creep effects.

Increasing R_a may also be disadvantageous from the point of view of pressure stresses and the resulting creep rates. Hence, none of these means seems appropriate to overcome the problems of high wall temperature without a penalty.

A slight beneficial effect which does not necessitate changing the module or coolant parameters may be expected from a reversal of the flow direction. This has already been indicated in Sec. 2. For a special case the differences are demonstrated in Fig. 5. The coolant temperature θ_c and wall temperature ϑ_o are plotted versus the angle φ as defined in Fig. 1. The curves shown are valid for $d = 0.5$ cm and $\alpha = 0.4$. Again it must be noted that the gain is small. It is of the order of the coolant temperature rise within the hemispherical gap.

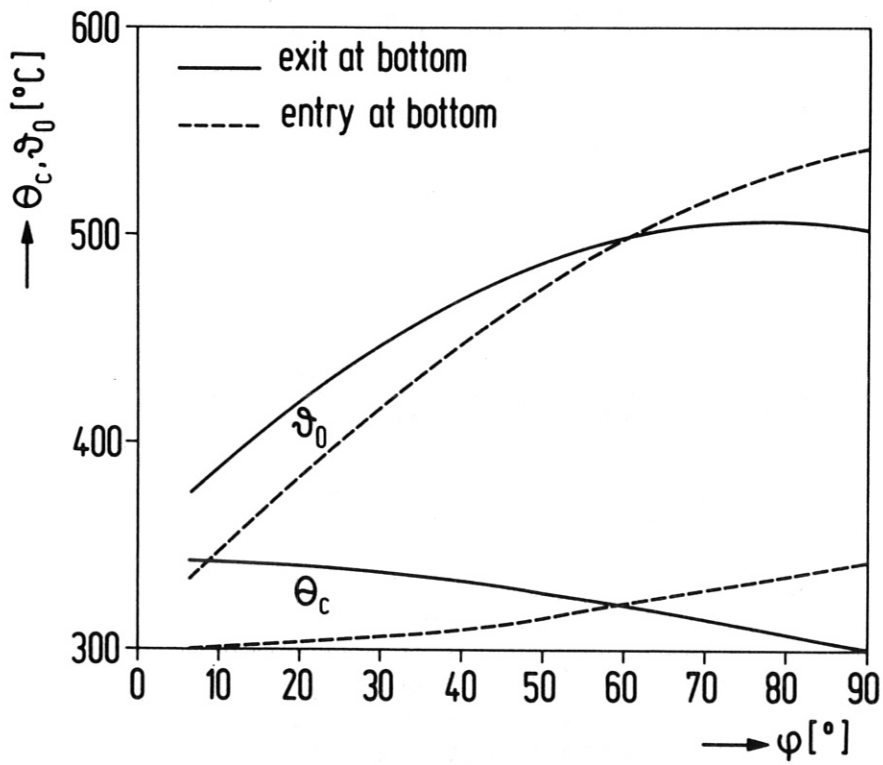

Fig. 5: Variation of the coolant temperature θ_c and the coolant-side wall temperature ϑ_o along the gap represented by the angle φ .

In conclusion, it has to be stated that the cooling concept investigated so far is not suitable for application in a wider parameter range with respect to wall thickness and fractional α-power. Although attractive because of its simplicity, it should only be envisaged in the case of low α-power delivered to the wall and negligible erosion rates.

5. The rectangular channel concept

The main disadvantage of the hemispherical annular gap concept analyzed and discussed in Sec. 4 is that the coolant velocity, which governs the heat transfer coefficient, varies over nearly one order of magnitude along the flow path. If the velocity were kept approximately constant, the problems could largely be relaxed.

A solution which satisfies this condition requires a constant flow cross-section. This can be accomplished by winding a channel within the cooling gap on the surface of the hemispherical cap as indicated in Fig. 6.

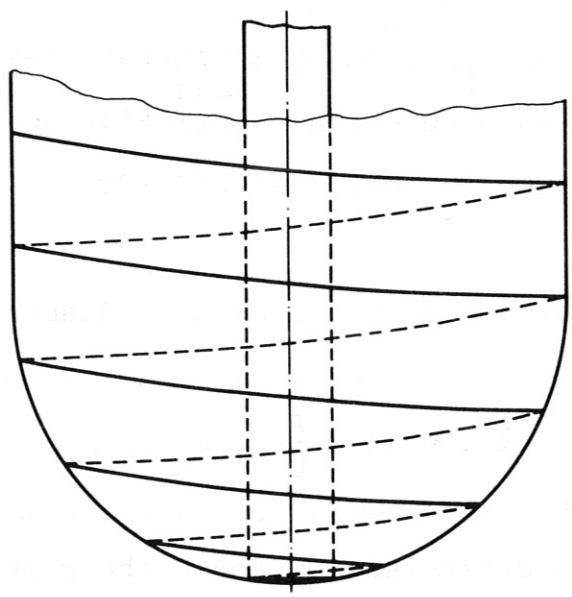

Fig. 6: Schematic representation of the rectangular channel concept.

Of course, this solution entails more expense from the manufacturing point of view and additionally dispenses with complete spherical symmetry as far as the temperature distribution is concerned. In spite of this, it is a step closer to the "cool-wall concept", it shows some flexibility in design, and it is relatively insensitive to the choice of the module size.

5.1. Analysis of the concept

For the following it is assumed that the coolant flow gap sketched in Fig. 6 may be considered as a rectangular channel. At some distance from the entry and exit regions its dimensions are assumed to be a and s as indicated in Fig. 7, where s is the channel width and a its height. Along both sides, denoted by a, constant heat flux densities are assumed which numerically agree with p_o and p_i as defined by eqs. (19) and (20).

From the definition of the hydraulic diameter

$$d_H = 4 \cdot \frac{A}{U} \quad , \tag{42}$$

where A is the cross-section and U the circumference of the channel, it follows that

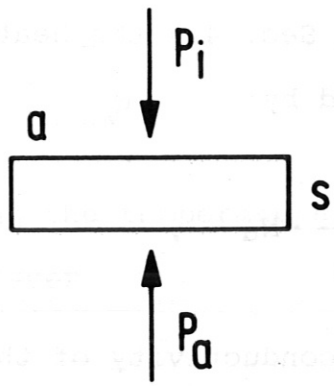

Fig. 7: Characteristic of the channel cross-section.

$$d_H = s \cdot \left(\frac{2 \cdot A_c}{1 + A_c} \right) . \tag{43}$$

With A_c the channel aspect ratio is introduced:

$$A_c = \frac{a}{s} . \tag{44}$$

The approximate length L of the channel can be calculated from the mean radius R_c of the hemispherical annular gap and the channel height a. Using the eq. (44), we obtain

$$L = \frac{2\pi \, R_c^2}{A_c \cdot s} . \tag{45}$$

We now consider first the heat transfer capability of the channel. As outlined in Sec. 4.1 the heat transfer coefficient h is defined by

$$h = \frac{k}{d_H} \cdot Nu \quad , \tag{46}$$

where k is the thermal conductivity of the coolant and the Nu the Nusselt number. The latter is given by the equation

$$Nu = 0.023 \cdot Re^{0.8} \cdot Pr^{0.4} \quad . \tag{47}$$

The Reynolds number Re and Prandtl number Pr are defined as

$$Re = \frac{w \cdot d_H \cdot \rho}{\mu} \quad , \tag{48}$$

$$Pr = \frac{c_p \cdot \mu}{k} \quad . \tag{49}$$

In these equations w denotes the coolant velocity, and ρ, μ, and c_p are the density, viscosity and specific heat of the coolant. If we introduce eqs. (48), (49), and (47) into eq. (46), we get

$$h = 0.023 \circ w^{0.8} \cdot d_H^{-0.2} \circ \rho^{0.8} \cdot c_p^{0.4} \circ k^{0.6} \circ \mu^{-0.4} \quad . \tag{50}$$

On the other hand, h is by definition

$$h = \frac{p_o}{\Delta \vartheta} \tag{51}$$

with $\Delta\vartheta$ denoting the temperature difference across the flow boundary layer.

By introducing eq. (51) into eq. (50) and resolving the equation for the terms containing the velocity w and the hydraulic diameter d_H we obtain

$$w^{0.8} \cdot d_H^{-02} = 43.478 \cdot \frac{p_o}{\Delta\vartheta \cdot f_1(\vartheta_F)} , \tag{52}$$

with the abbreviation

$$f_1(\vartheta_F) = \rho^{0.8} \cdot c_p^{0.4} \cdot k^{0.6} \cdot \mu^{-0.4} . \tag{53}$$

This temperature function containing coolant property values only has to be evaluated for the mean film temperature ϑ_F given by eq. (39). If in eq. (52), we replace d_H by the expression (43), we obtain

$$w^{0.8} \cdot s^{-0.2} \cdot \left(\frac{2 \cdot A_c}{1 + A_c} \right)^{-0.2} = 43.478 \cdot \frac{p_o}{\Delta\vartheta \cdot F_1(\vartheta_F)} \tag{54}$$

This equation describes a first relation between the coolant velocity and the channel characteristics which has to be satisfied in order to ensure a certain temperature difference $\Delta\vartheta$ being maintained between the wall and coolant.

A second relation follows from the overall power balance of the module:

$$P_{th} = (p_o + p_i) \cdot 2\pi R_c^2 \cdot \frac{1}{\beta} = m \cdot c_p \cdot \Delta\theta \qquad (55)$$

In this notation it is assumed that $s << R_c$; β follows from eq. (14). The mass flow rate $\dot{m}$ can be expressed by

$$\dot{m} = w \circ A \cdot \rho = w \circ s^2 \cdot A_c \circ \rho \qquad (56)$$

By substituting eq. (56) in eq. (55) and resolving the equation again for w, s, and A_c we obtain

$$w \cdot s^2 \cdot A_c = \frac{2\pi R_c^2 (p_o + p_i)}{\beta \circ \Delta\theta \cdot f_2(\bar{\theta}_c)} , \qquad (57)$$

with the abbreviation

$$f_2(\bar{\theta}_c) = \rho \circ c_p . \qquad (58)$$

In contrast to eq. (53), here the mean coolant temperature $\overline{\vartheta}_c$ is the appropriate temperature for evaluating the coolant property data:

$$\overline{\vartheta}_c = \vartheta_i + 0.5 \cdot \beta \cdot \Delta\vartheta \quad . \tag{59}$$

In order to obtain a consistent solution for w, s, and A_c, a third equation is needed. It can be supplied by considering the pressure loss over the channel length or the necessary pumping power. The pressure loss Δp generally obeys the Blasius equation

$$\Delta p = \lambda \cdot \frac{L}{d_H} \cdot \frac{\rho}{2} w^2 \quad . \tag{60}$$

In the case of turbulent coolant flow the friction coefficient λ for a smooth pipe is given by

$$\lambda = 0.3164 \quad Re^{-0.25} \tag{61}$$

From eqs. (60) and (61) we get

$$\Delta p = 1.582 \cdot 10^{-8} \cdot w^{1.75} \cdot d_H^{-1.25} \cdot L \cdot \rho^{0.75} \cdot \mu^{0.25} \quad [MPa] \tag{62}$$

If we use the abbreviation

$$f_3(\vartheta_F) = \rho^{0.75} \cdot \mu^{0.25} \tag{63}$$

and replace d_H and L by eqs. (43) and (45), we finally arrive at the relation

$$w^{1.75} \cdot s^{-2.25} \cdot \frac{1}{A_c} \left(\frac{2 \cdot A_c}{1 + A_c}\right)^{-1.25} = 1.006 \cdot 10^7 \cdot \frac{\Delta p}{R_c^2 \cdot f_3(\mathfrak{F}_F)} \quad . \tag{64}$$

As can be seen from this equation, its evaluation calls for a knowledge of the acceptable pressure loss Δp. Alternatively, the acceptable pumping power could be prescribed. The pumping power P_p is given by

$$P_p = \Delta p \cdot \frac{\dot{m}}{\rho_i} \quad , \tag{65}$$

where ρ_i is the coolant density at inlet temperature conditions. From eq. (55) $\dot{m}$ can be expressed by

$$\dot{m} = \frac{P_{th}}{c_p \cdot \Delta\theta} \quad . \tag{66}$$

Combining eqs. (65) and (66) yields as a rather informative quantity the fractional pumping power ε_p :

$$\varepsilon_p = \frac{P_p}{P_{th}} = \frac{\Delta p}{\rho_i \cdot c_p \cdot \Delta\theta} \quad . \tag{67}$$

According to eq. (58) we abbreviate

$$f_2(\theta_i) = \rho_i \cdot c_p \tag{68}$$

and obtain for Δp

$$\Delta p = \varepsilon_p \cdot \Delta\theta \cdot f_2(\theta_i) \quad . \tag{69}$$

Hence, as an equivalent to eq. (64) it is possible to use the following relation:

$$w^{1.75} \cdot s^{-2.25} \cdot \frac{1}{A_c} \left(\frac{2 \cdot A_c}{1 + A_c} \right)^{-1.25} = 1.006 \cdot 10^7 \cdot \frac{\varepsilon_p \cdot \Delta\theta \cdot f_2(\theta_i)}{R_c^2 \cdot f_3(\vartheta_F)} \tag{70}$$

With eqs. (54), (57), and (64) or (70) three equations are available which provide a consistent solution for w, s, and A_c. We now introduce the following abbreviations for the right-hand sides of eqs. (70), (57), and (54):

$$A_o = 1.006 \cdot 10^7 \frac{\varepsilon_p \cdot \Delta\theta \cdot f_2(\theta_i)}{R_c^2 \cdot f_3(\vartheta_F)} \tag{71}$$

$$B_o = \frac{2\pi R_c^2 \cdot p_o (1 + p_i/p_o)}{\beta \cdot \Delta\theta \circ f_2(\bar{\theta}_c)} \tag{72}$$

$$C_o = 43.478 \frac{p_o}{\Delta\vartheta \cdot f_2(\lambda_F)} \tag{73}$$

We thus obtain

$$w^{1.75} \; s^{-2.25} \; \frac{1}{A_c} \left(\frac{2 \cdot A_c}{1 + A_c} \right)^{-1.25} = A_o \tag{74}$$

$$w \cdot s^2 \cdot A_c = B_o \tag{75}$$

$$w^{0.8} \cdot s^{-0.2} \cdot \left(\frac{2 \cdot A_c}{1 + A_c} \right)^{-0.2} = C_o \cdot \tag{76}$$

From eq. (75) we get

$$w = \frac{B_o}{s^2 \cdot A_c} \cdot \tag{77}$$

Replacing w in eq. (76) by eq. (77) yields

$$s = \left[\frac{B_o^{0.8}}{C_o} \cdot A_c^{-0.8} \left(\frac{2 \cdot A_c}{1 + A_c} \right)^{-0.2} \right]^{\frac{1}{1.8}} \tag{78}$$

and

$$w = \frac{B_o}{A_c} \left[\frac{B_o^{0.8}}{C_o} \cdot A_c^{-0.8} \left(\frac{2 \circ A_c}{1 + A_c} \right)^{-0.2} \right]^{-\frac{1}{0.9}} \tag{79}$$

By introducing eqs. (78) and (79) into eq. (74) we finally get

$$A_c^{-0.1945} \cdot \left(\frac{2 \cdot A_c}{1 + A_c} \right)^{-0.6111} = \frac{A_o \, B_o^{0.8055}}{C_o^{3.1944}} \, . \qquad (80)$$

For prescribed conditions defining A_o, B_o, and C_o we can now find the channel aspect ratio if we know

$$g(A_c) = A_c^{-0.1945} \cdot \left(\frac{2 \, A_c}{1 + A_c} \right)^{-0.6111} \, . \qquad (81)$$

With A_c found from this procedure we can find the channel width s and the coolant velocity w from eqs. (78) and (79). Thus, a consistent solution for these variables is obtained which satisfies the prescribed values for R_c, $\Delta\Theta$, β, p_o, p_i, $\Delta\vartheta$, and ε_p.

Figure 8 shows the function $g(A_c)$ for A_c values of interest, subdivided in the ranges $A_c \leq 1$ (Fig. 8a) and $A_c \geq 1$ (Fig. 8b). $A_c = 1$ corresponds to a channel of square cross-section. Low values for $g(A_c)$ can obviously only be reached if A_c is chosen as $A_c > 1$, which means a channel in which the height a is larger than the width s. Since according to eqs. (80) and (73)

$$g(A_c) \sim \Delta\vartheta^{3.1944} \, , \qquad (82)$$

high values for A_c are necessary to obtain low temperature differences between the wall and coolant. The third-order dependence additionally indicates the very high sensitivity.

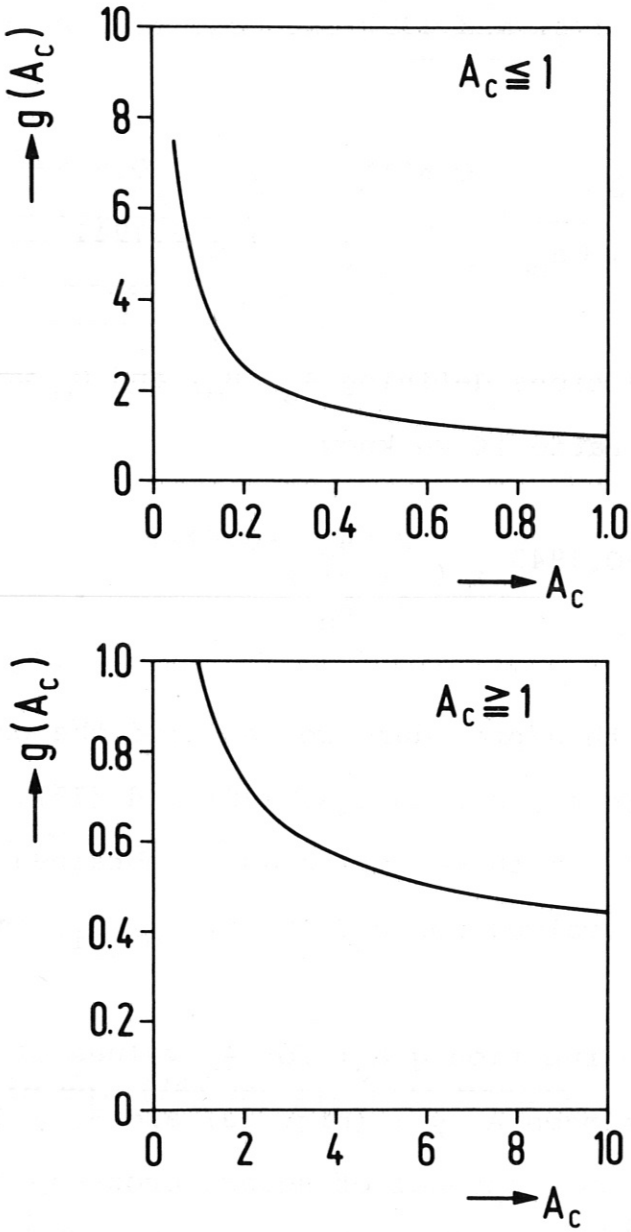

Fig. 8: The function $g(A_c)$ as defined by eq. (81) for channel aspect ratios $A_c \leq 1$ (a) and $A_c \geq 1$ (b).

With regard to numerical evaluations this high sensitivity is inappropriate in that easily A_c values far from reality are calculated if the restriction on $\Delta\vartheta$ is chosen too strong. For example, the conditions $\alpha = 1.0$; $d = 1.5$ cm; $R_a = 5$ cm; $\theta_i = 300^{\circ}C$; $\theta_o = 500^{\circ}C$; $p_c = 4$ MPa; and $\varepsilon_p = 0.01$, which result in $\beta = 0.36$; $p_o = 96$ W/cm^2; $p_i = 7.5$ W/cm^2, and $R_c \approx 3.4$ cm lead to a value of $A_c > 10^8$ if $\Delta\vartheta$ is to be restricted to $\Delta\vartheta = 50^{\circ}C$.

For practical calculations it is therefore more reasonable to evaluate eq. (80) by prescribing A_c and calculating $\Delta\vartheta$ instead. $\Delta\vartheta$ then determines the value of C_o which together with A_c can be used to find s and w from eqs. (78) and (79), which belong to the consistent set of parameters. If we do so, we arrive at the following equations for $\Delta\vartheta$, s, and w:

$$\Delta\vartheta = 0.1759 \cdot G_1(A_c) \cdot \frac{p_o^{0.7479} \cdot R_c^{0.1218}}{f_1(\vartheta_F) \cdot \Delta\theta^{0.0609}} \cdot \left[\frac{f_3(\vartheta_F)}{\varepsilon_p \cdot f_2(\theta_o)}\right]^{0.3130} \cdot \left[\frac{\beta \cdot f_2(\bar{\theta}_c)}{(1 + \frac{p_i}{p_o})}\right]^{0.2521}, \tag{83}$$

$$s = 0.2783 \cdot G_2(A_c) \cdot \frac{R_c^{0.8888}}{p_o^{0.1112}} \cdot \left[\Delta\vartheta \cdot f_1(\vartheta_F)\right]^{0.5556} \cdot$$

$$\left[\frac{(1 + \frac{p_i}{p_o})}{\beta \cdot \Delta\Theta \cdot f_2(\bar{\Theta}_c)}\right]^{0.4444} \tag{84}$$

$$w = 81.103 \cdot G_3(A_c) \cdot p_o^{1.2223} \cdot R_c^{0.2224} \cdot$$

$$\cdot \frac{\left[\frac{(1 + p_i/p_o)}{\beta \cdot \Delta\Theta \cdot f_2(\bar{\Theta}_c)}\right]^{0.1112}}{\left[\Delta\vartheta \cdot f_1(\vartheta_F)\right]^{1.1111}} \cdot \tag{85}$$

The influence of the channel aspect ratio A_c is now given by the three functions $G_1(A_c)$, $G_2(A_c)$, and $G_3(A_c)$, which read

$$G_1(A_c) = 0.8758 \cdot A_c^{-0.2522} \cdot (1 + A_c)^{0.1913} \tag{86}$$

$$G_2(A_c) = 0.9259 \cdot A_c^{-0.5556} \cdot (1 + A_c)^{0.1111} \tag{87}$$

$$G_3(A_c) = 1.1665 \cdot A_c^{0.1111} \cdot (1 + A_c)^{-0.2222} \tag{88}$$

They are shown in Figure 9. As can be seen from this figure, the choice of the channel aspect ratio A_c significantly influences the channel width s, while it only has a weak effect on the coolant velocity w. The influence of A_c on the temperature difference $\Delta\vartheta$ tends to saturation at higher values of A_c. This puts an upper limit on A_c above which no practical improvement can be expected.

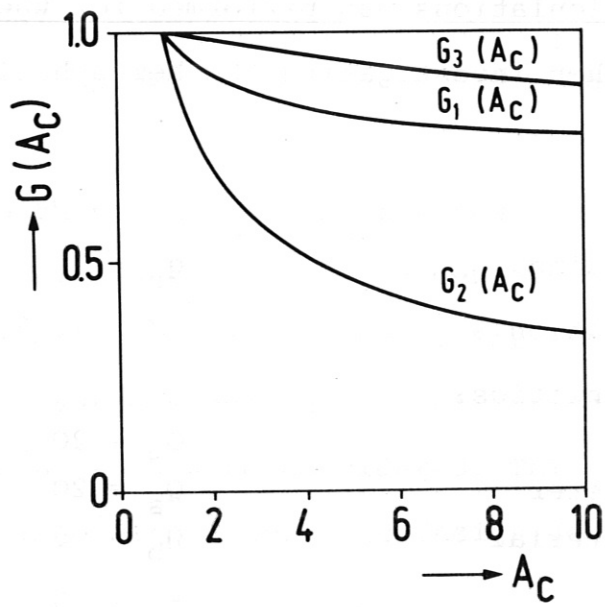

Fig. 9: The functions $G(A_c)$ as defined by eqs. (80), (87), and (88) for channel aspect ratios $A_c > 1$.

5.2. Numerical results

Utilizing eqs. (83) to (88) for evaluating numerical results require, of course, some iterative procedure with respect to the temperatures and the mean channel radius. However, this procedure converges rather rapidly. Furthermore, we dispense with adjustment of the heat flux density, which is only a weak function of s.

A first series of calculations was performed for the same fixed parameters as used when investigating the hemispherical annular gap concept:

Neutron wall loading	$q_n = 2$	MW/m^2
Energy multiplication	$M = 1.13$	
Nuclear power densities:		
- First wall	$Q_w = 20$	W/cm^3
- Second canister	$Q_s = 20$	W/cm^3
- Breeding material	$Q_b = 6$	W/cm^3
Module radius	$R_a = 5$	cm
Thickness of 2nd canister	$d_s = 0.1$	cm
Radius of central pipe	$r_e = 0.5$	cm
Coolant pressure	$p_c = 4$	MPa
Inlet temperature	$\theta_i = 300^{\circ}C$	
Outlet temperature	$\theta_o = 500^{\circ}C$	
Relative pressure loss	$\Delta p/p_c = 0.01$	

From the latter value an actual pressure loss of $\Delta p_c = 0.04$ MPa is obtained, which seems small enough to neglect the influence of pressure level variations along the coolant channel. Owing to eq. (67) this gives rise to a relative pumping power of 1.15 %.

Again we varied the fraction α of the α-power delivered to the wall and the first-wall thickness d in the following ranges:

Fractional α-power	α = 0. to 1.0
First-wall thickness	d = 0.2 to 1.6 cm

According to these parameters, the power contribution of the module head, β, and the heat flux densities p_o and p_i were chosen as given in Figures 2 and 3. For each parameter combination various channel aspect ratios A_c ranging from $A_c = 1$ up to $A_c = 15$ were considered. This seems to be a reasonable range with respect to design feasibility.

Figure 10 shows, for the four corners of the parameter ranges of α and d, the variation of the resulting wall temperature ϑ_o with A_c. This figure clearly demonstrates that the choice of the channel aspect ratio only becomes important in the case of thick walls and high α-power delivered to the wall.

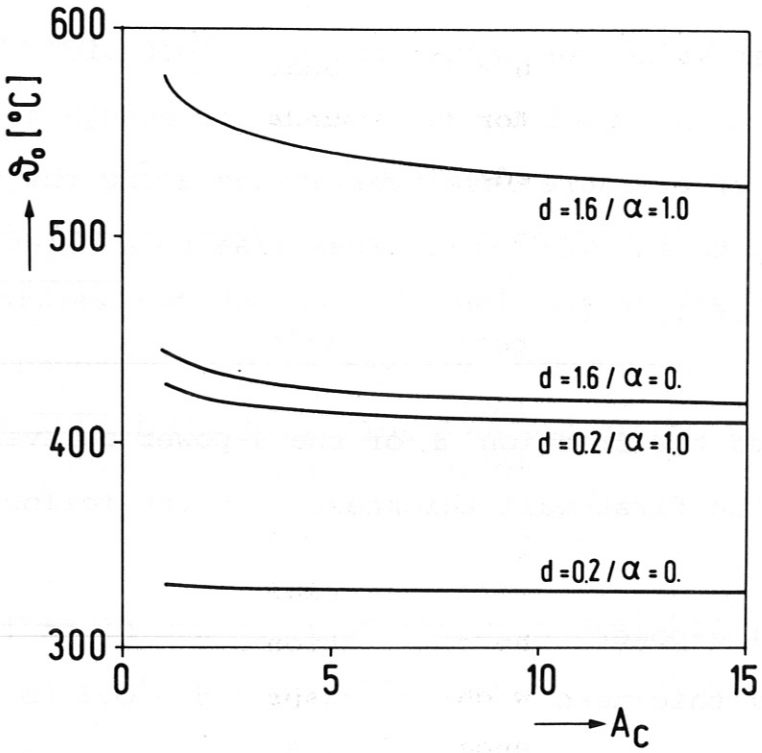

Fig. 10: The coolant side wall temperature ϑ_o as a function of the channel aspect ratio A_c for the boundaries of the parameter range investigated.

Figure 11 shows the corresponding variation of the channel width s. It is, as already suggested by the variation of $G_2(A_c)$ (see Fig. 9), a stronger function of A_c. The other parameters only have a weak impact. The minimum value of about 0.2 cm does not seem unreasonable either from the manufacturing point of view. In fact, it proves to be even larger than that assumed for the hemispherical annular gap concept, which raised major difficulties with respect to the wall temperatures.

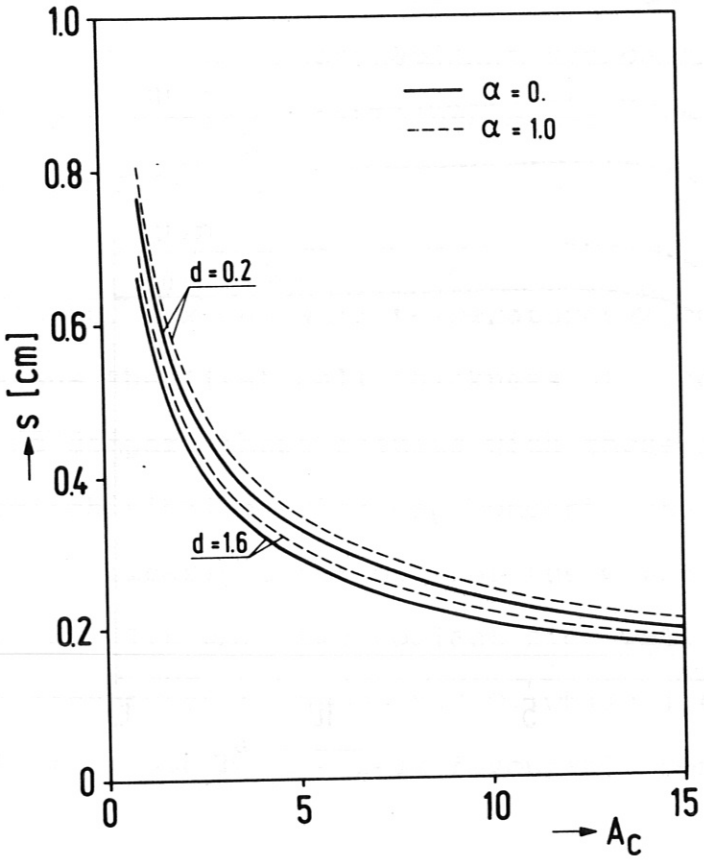

Fig. 11: The channel width s as a function of the channel aspect ratio A_c for the boundaries of the parameter range investigated

In Figure 12, finally, the variation of the coolant velocity with A_c is shown. The interesting result here is the occurance of a weak maximum which coincides with a similarly weak minimum in the flow cross-section. It is located near $A_c = 4$. This feature is, at first glance, in contradiction with the variation of $G_2(A_c)$ (see Fig. 9). It can be explained, however, with the adjustment of R_c during the calculation. Since R_c is dependent on s, and s is large at low channel aspect ratios A_c, this effect overrides the direct influence via $G_3(A_c)$.

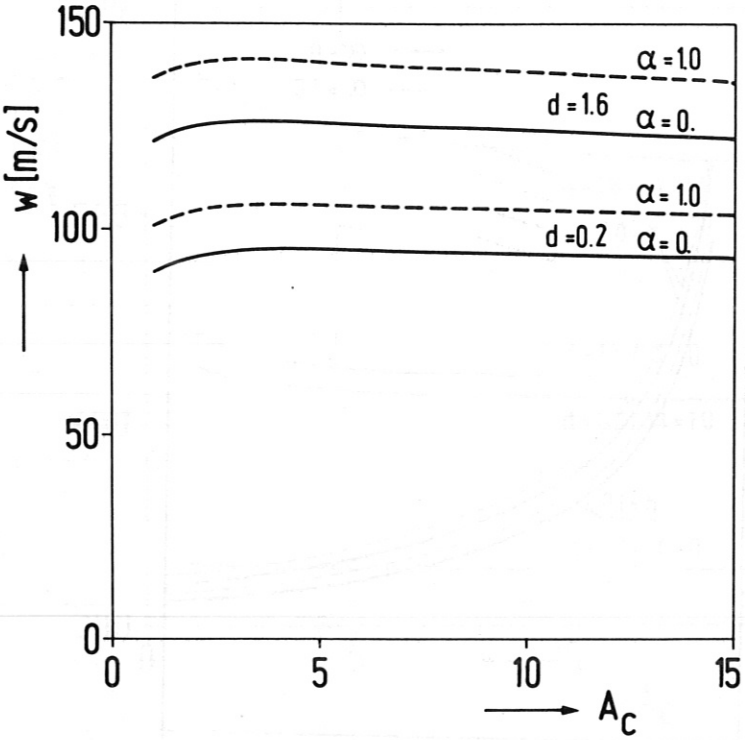

Fig. 12: The coolant velocity w as a function of the channel aspect ratio A_c for the boundaries of the parameter range investigated.

The results discussed so far show no clear preference for the appropriate choice of A_c, irrespective of the requirement that it be made as large as possible. Rather must a decision therefore be taken on practical grounds. If, for instance, we put a lower limit of s_{min} = 0.2 cm on the channel width, we learn from Fig. 11 that the channel aspect ratio should not exceed A_c = 10, at least in the case of thick walls. This means that the channel has about three windings around the hemisphere.

While this assumption is reasonable with regard to high values of α and d, it is not unreasonable in the case of lower values. In the following we shall therefore compare the results for this specific value of A_c.

In Figure 13 the maximum wall temperatures ϑ_o obtained are plotted versus the first-wall thickness d for various values of α. If we compare these results with those in Fig. 4 valid for the hemispherical annular gap concept, the channel concept is found to be clearly superior. For the worst case considered (α = 1.0 ; d = 1.6 cm) the coolant side wall temperature ϑ_o can now be restricted to about 530°C, while 1140°C had to expected in the case of the less favourable concept.

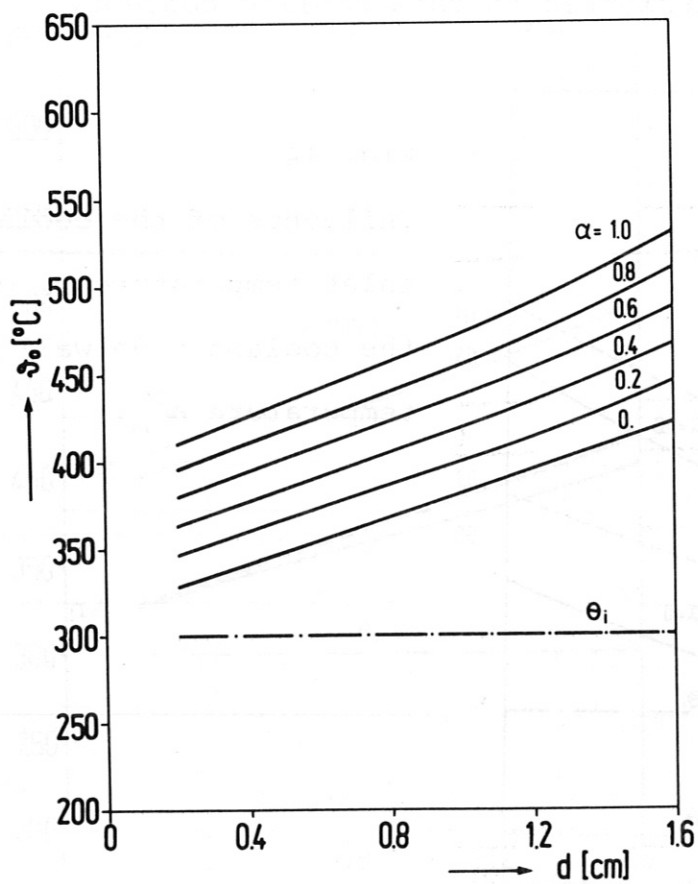

Fig. 13:
The coolant side-wall temperature ϑ_o as a function of the wall thickness d and the fractional α-power α for the case of $A_c = 10$.

Further improvements could be achieved by modifying the cooling conditions. If, for instance, the coolant inlet temperature Θ_i is decreased to 230°C instead of 300°C, a gain in ϑ_o of at least 35°C is obtained, as shown in Fig. 14. The wall temperature can thus be assumed not to exceed 500°C. As demonstrated in Figure 15 and 16, similar conditions could be achieved either if the coolant pressure is raised to about 6 MPa or if the relative pressure loss allowed to occur along the channel is doubled as compared with the reference value. Although these gains are not higher in absolute numbers, they are more profitable here than in the hemispherical annular gap concept. Furthermore an increase of the module size does not lead to deleterious results. Assuming $R_a = 10$ cm results in temperatures of about 20°C higher than in the case of $R_a = 5$ cm. Hence, much more flexibility can be attributed to this cooling concept.

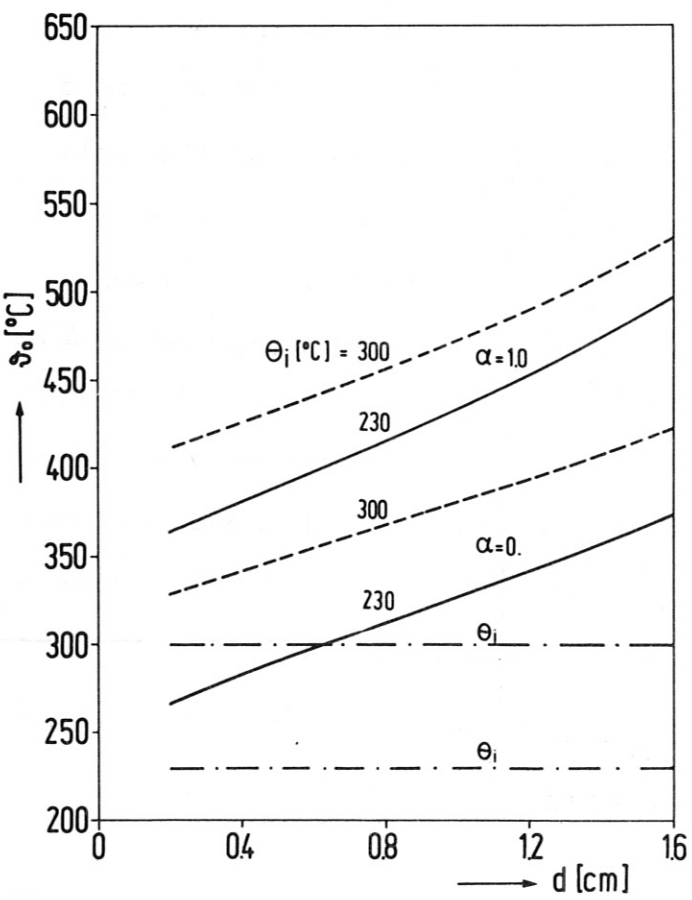

Fig. 14:
Influence of the coolant inlet temperature Θ_i on the coolant side-wall temperature ϑ_o.

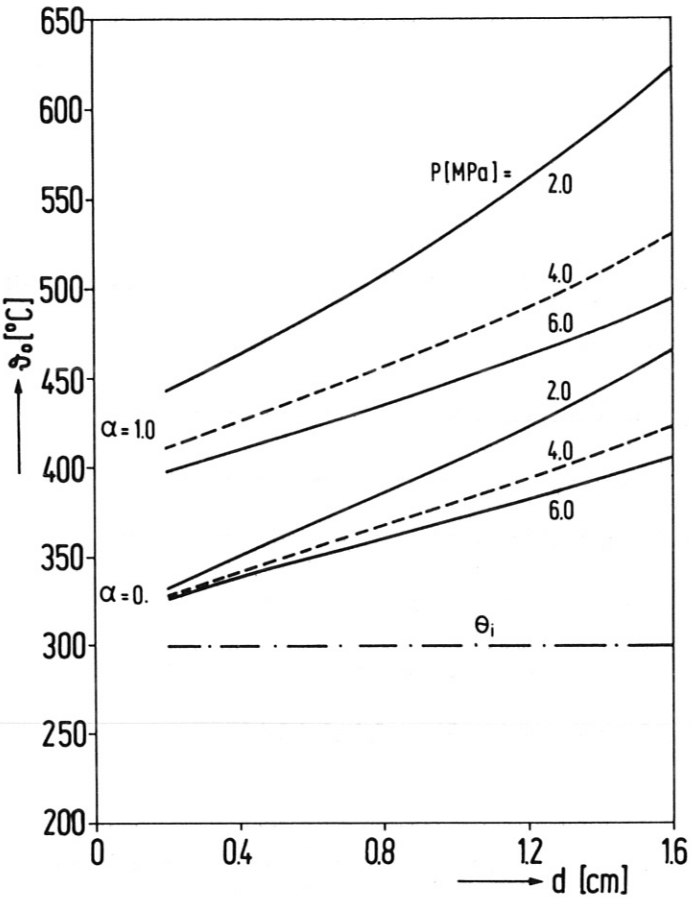

Fig. 15:
Influence of the coolant pressure P on the coolant-side wall temperature ϑ_o.

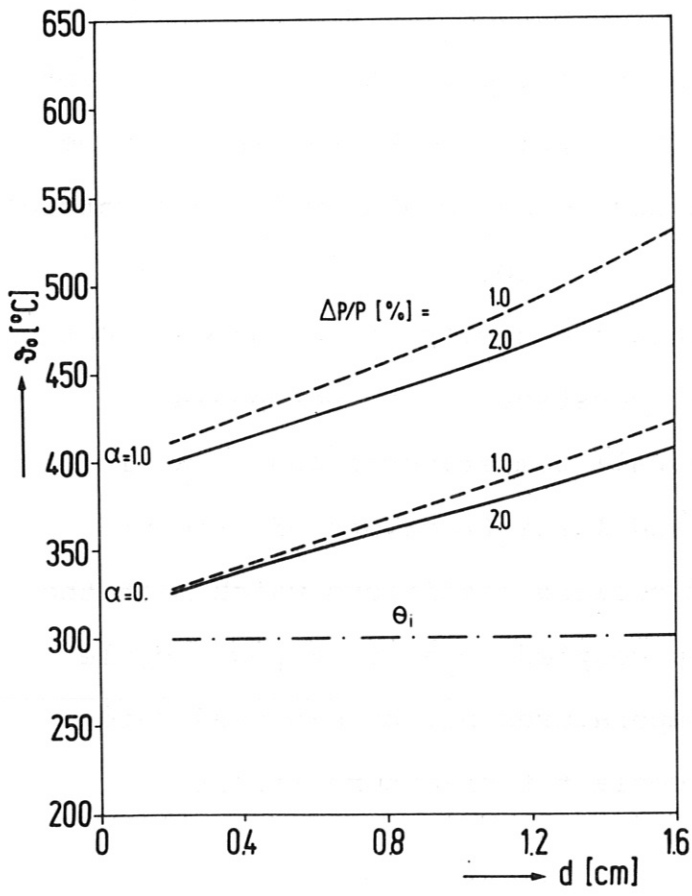

Fig. 16:
Influence of the allowed relative pressure loss ΔP/P on the coolant-side wall temperature ϑ_o.

6. Conclusions

The purpose of this study was to investigate whether the concept of a "cool wall" can be realized with a cylindrical module closed by a hemispherical cap and using helium gas as the coolant. The advantage of this type of module is that it allows relatively simple analysis of its mechanical performances, including the lifetime under fusion reactor irradiation. Considered from this point of view, the results obtained point to a high degree of consistency and reliability.

The results demonstrated that the simplest approach to cooling the first wall - the hemispherical annular gap concept - does not meet the requirements of a "cool wall" over the entire parameter range considered. Only if the first wall can be kept thin and the fraction of α-power delivered to the wall can be kept small, can this concept ensure acceptable wall temperatures.

If the coolant is guided within the hemispherical gap so that its velocity is approximately constant - the rectangular channel concept - acceptable wall temperatures can be achieved up to high wall thicknesses and large fractions of α-power delivered to the wall. Under cooling conditions which meet the requirements of a helium loop coupled to a steam power cycle maximum coolant side wall temperatures may be expected which are within the range of the coolant temperature itself.

Admittedly, it is doubtful whether temperatures of 300°C to 500°C fit into the idea of a cool wall. On the other hand, it must be strongly questioned whether such an idea can really be maintained unless the first wall is relieved of its task of coping with the direct energy and particle impact from the plasma.

References

[1] INTOR: International Tokamak Reactor, Phase IIa:
Conclusion from the 3rd Workshop Meeting;
Commission of the European Communities,
EURFUBRU / XII-2 / 81/ EDV 80 , Dec. 1982

[2] INTOR: International Tokamak Reactor, Phase IIa:
European Contributions to the 4th Workshop Meeting;
Commission of the European Communities,
EURFUBRU / XII-132 / 82 / EDV 10 , March 1982

[3] W. Daenner: "Some nuclear characteristics of liquid-lithium, stainless-steel fusion reactor blankets",
IPP report (under preparation)

[4] W. Zimmerer: "MAPLIB - Funktionen zur Berechnung der Zustandsgrößen von Helium, Luft Kohlendioxid und Wasser",
KFK 1403 (1971)